Materials Today Communications 31 (2022) 103642

Contents lists available at ScienceDirect

Materials Today Communications

journal homepage: www.elsevier.com/locate/mtcomm

Molecular dynamics simulation of perforation of graphene under impact by fullerene projectiles

Yang Zhang [a,b], Yun Qiu [a], Fuzhou Niu [c], A.S. Ademiloye [d,*]

[a] School of Science, Nanjing University of Science and Technology, Nanjing 210094, China
[b] Department of Architecture and Civil Engineering, City University of Hong Kong, Kowloon, Hong Kong, China
[c] School of Mechanical Engineering, Suzhou University of Science and Technology, Suzhou 215009, China
[d] Zienkiewicz Centre for Computational Engineering, Faculty of Science and Engineering, Swansea University Bay Campus, Swansea SA1 8EN, UK

ARTICLE INFO

Keywords:
Molecular dynamics
Perforation
Fullerene projectile
Buckling characteristics
Ballistic limit velocity
Impact protection

ABSTRACT

In this paper, molecular dynamics (MD) simulations are employed to study the perforation of graphene under impact by fullerenes of various sizes. The buckling characteristics of fullerenes after impact are classified and discussed. The relative state of C_{180} projectile and graphene under impact at different velocities is also investigated. We observed that the C_{180} projectile rebounds at low velocity ($V < 4.25$ km/s), sticks to graphene at high velocity (4.25 km/s $\leq V \leq$ 4.75 km/s), and perforates the graphene at higher velocity ($V \geq 4.75$ km/s). It is found that the buckled cap of large-size fullerene formed after impact can better absorb kinetic energy. In addition, different crack modes of graphene after perforation were investigated. The effect of fullerene projectile size and initial velocity on ballistic limit velocity was also clarified. This study provides new implications for the application of large-size fullerenes as impact shields.

1. Introduction

Protecting equipment and structures from penetration under high-energy impact is a challenging problem in theoretical and experimental research, which involves various fields of applied technology including material science and engineering, aerospace and automotive, such as armor materials [1], high hardness armor steel [2] and orbiting debris shield [3,4]. With the advent of the nanomaterial era, 2D materials (such as graphene) have developed rapidly due to their extremely good mechanical properties. Graphene, the perfect two-dimensional lattice of sp^2-bonded carbon atoms [5], has excellent mechanical properties [6–8], namely high Young's modulus (1 TPa), high ultimate strength (130 GPa [9]), and low density (2200 kg.m^{-3}). Graphene is very good for overcoming the limitations of some traditional materials [10,11]. Their excellent potential as an energy absorption material has attracted great attention. Several researchers have confirmed the feasibility of using graphene and its family branches – 0-dimensional fullerene, 1-dimensional nanotubes, 3-dimensional graphite [12] – as a ballistic protection material [13–15]. This ability makes it a suitable candidate material for the desired breakthrough in impact protection [16].

In comparison to the huge number of experimental testing and finite element studies that have been carried out on the impact load response of traditional composite materials [17–19], the impact properties of nanomaterials, especially graphene, and nanocomposites are rarely reported theoretically [20,21]. It has been established that graphene can effectively improve the properties of nanocomposites [22–26]. Ávila et al. [27] reported that the addition of graphene to conventional composites can improve their impact resistance. Lee et al. [28] conducted a microballistic test on the multilayer graphene with thickness between 10 nm and 100 nm. After the impact of a high-velocity projectile, the impacted area of graphene is stretched into a cone. In addition, the authors observed that the generated radial crack expanded outward and exceeded the impact area. They also observed that the penetration energy of multilayer graphene is more than 10 times that of a steel plate.

In 2013, Xu et al. [29] studied the dynamic impact response of a series of buckyballs using MD simulation. The potential energy of the unrecoverable buckle structure is the main source of energy absorption. Their experiments revealed the energy dissipation potential of the buckyballs under various impact energies. Through a combination of numerical simulation and theoretical modeling, Bizao et al. [30] studied the scale effect of ballistic penetration of graphene sheets, clarified the role of defects in the process of graphene penetration, and found the

* Corresponding author.
E-mail address: a.s.ademiloye@swansea.ac.uk (A.S. Ademiloye).

https://doi.org/10.1016/j.mtcomm.2022.103642
Received 5 January 2022; Received in revised form 12 April 2022; Accepted 1 May 2022
Available online 6 May 2022

failure mechanism of graphene sheets. Their numerical results showed that the specific energy penetration value is extremely high, which is an order of magnitude larger than the experimentally measured value. MD simulation technique has also been employed to investigate the mechanical properties of C_{720} under quasi-static and dynamic impact [31]. Here, the authors observed that the unit energy absorption density of low-velocity impact wave is the same regardless of the number of buckyballs. Under different stacking forms, stacking density and impact velocity of C_{720} were found to have a positive impact on unit energy absorption.

Meng et al. [32] observed and studied the size effect of graphene film caused by conical wave reflection under ballistic trajectory for the first time through simulation and theoretical model. This theoretical analysis fills the gap in the finite film behavior during the projectile impact. Their results showed that the key relationship between film size and projectile size only depends on film thickness and film density ratio. More recently, Qiu et al. [33] investigated the behavior of single-layer and rotated double-layer graphene sheets under a high velocity impact using MD simulations. Based on the high cone-wave and axial-wave velocities observed in their numerical simulations, the authors concluded that single-layer and double-layer graphene sheets have potential applications in impact protection materials.

Thus far, there are few studies on large-size fullerenes perforating graphene and corresponding ballistic limit impact characteristics. In this paper, the MD technique is used to simulate the impact of fullerenes with different sizes on graphene in order to study their buckling characteristics and examine the perforation behavior of graphene. Firstly, the buckling characteristics of fullerenes impacting graphene are studied, and the buckling deformation during impact is visualized. Subsequently, we study the fracture and perforation behavior of graphene under the impact of C_{180} projectile and analyze its crack mode. Finally, we study the effect of fullerene projectile velocity and radius on the ballistic limit velocity.

2. Simulation method

In this study, the Large-scale Atomic/Molecular Massively Parallel Simulator (LAMMPS) [34] package is used for all simulations, and visualization of atoms is achieved using Visual Molecular Dynamics (VMD) [35]. The Adaptive Intermolecular Reactive Empirical Bond Order (AIREBO) [36] force field is used to study intramolecular and intermolecular interactions. Graphene and fullerenes of various sizes are composed of carbon atoms. AIREBO potential is widely used to study the mechanical properties of carbon systems. We employed the Nose-Hoover thermostat [37] to relax the simulation system 5 ps, select step of 0.5 fs for simulation, consider the system temperature of 1 K, and apply the NVE ensemble for impact simulations.

Fullerene projectile is used to impact monolayer graphene. Fullerenes are spherical, which is convenient for theoretical calculations and simplified models. In our simulation, all four edges of the graphene sheet are fixed (Fig. 1a). Fullerene projectile is located in the middle of graphene, and its center has sufficient initial distance from the graphene center to avoid any interaction between fullerene atoms and graphene atoms as illustrated in Fig. 1(b). The cutoff function in AIREBO potential field is given in Eq. (1) [38]:

$$f(r) = \begin{cases} 1, & r < R^{(1)} \\ \frac{1}{2}\left[1 + \cos\left(\frac{\pi\left(r - R^{(1)}\right)}{R^{(2)} - R^{(1)}}\right)\right], & R^{(1)} < r < R^{(2)} \\ 0, & r > R^{(2)} \end{cases} \quad (1)$$

where r is the bond length, $R^{(1)}$ and $R^{(2)}$ are the cutoff radii, taken as 1.7 Å and 2.0 Å, respectively. Some researchers used the improved cutoff radii of 1.92 Å and 2.0 Å to eliminate the nonphysical behavior in the simulation [39]. The authors of Ref. [40] studied the effect of cutoff function on graphene fracture simulation and found that when the $R^{(1)}$ and $R^{(2)}$ are equal to 2 Å, the nonphysical behavior in the simulation disappears, and it can capture the breaking of bond more accurately during impact.

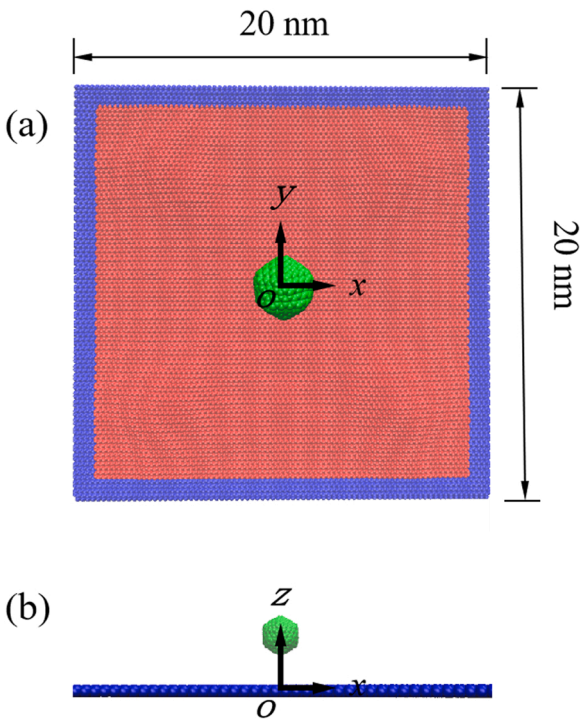

Fig. 1. Schematic of the impact simulation setup. The blue regions represent the fixed boundaries.

3. Results and discussions

3.1. Buckling characteristics of fullerenes

In order to study the buckling characteristics of fullerenes, the simulation system consists of fullerenes of various sizes and a graphene sheet with a dimension of 20 nm × 20 nm. Seven fullerenes with different diameters are selected in this simulation, which were generated using the Nanotube Modeler program [41]. Their schematics and physical parameters are shown in Fig. 2, and Table 1 respectively.

The velocity of fullerene is set to 3 km/s to initiate the impact process. This velocity value was selected to ensure that the structure of the graphene sheet remains intact without any cracks or perforations during the impact process [42]. The kinetic energy of the fullerene during impact is monitored, and the configuration of the projectile in the buckling stage is shown. An important parameter for evaluating fullerene energy absorption is specific energy absorption (SEA), which is computed using $\left(E_{impact} - E_{rebound}\right)/M$, where E_{impact} is initial kinetic energy of the fullerene, $E_{rebound}$ is residual kinetic energy of the fullerene and M is the mass of the fullerene given in Table 1. The SEA of fullerene is transferred to the graphene sheet and converted into the kinetic and potential energies of the graphene sheet.

As shown in Fig. 3, buckling characteristics of fullerenes during impact can be divided into three categories: type I occurs only in the C_{60} fullerene – it involves only slight compressed deformation without any buckling, and it can be attributed to the greater "stiffness" of the C_{60} fullerene. Type II occurs in $C_{180} \sim C_{320}$ fullerenes – it is characterized by obvious buckling during the impact process and the system reaches the maximum potential energy state for a hollow elastic sphere [43]. Here, the fullerene buckles when compressed and a part of the sphere is inverted. In the rebound stage, deformation recovers, which makes the

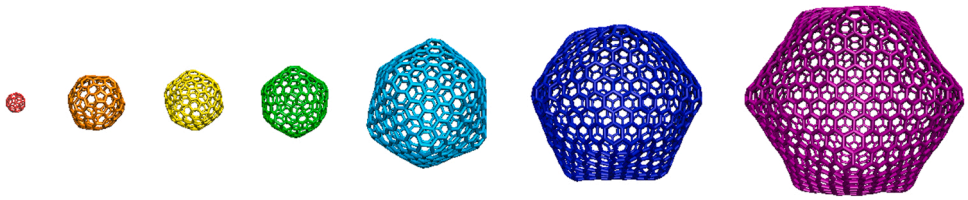

Fig. 2. Schematic of C_{60} - C_{1500} molecules.

Table 1
Physical parameters of C_{60} - C_{1500} molecules [41].

Fullerene	Diameter, D (Å)	Mass, M (g)
C_{60}	6.9	1.19E-21
C_{180}	12	3.58E-21
C_{240}	13.8	4.77E-21
C_{320}	16.4	6.47E-21
C_{540}	21.2	1.08E-20
C_{960}	27.2	1.91E-20
C_{1500}	33.9	2.99E-20

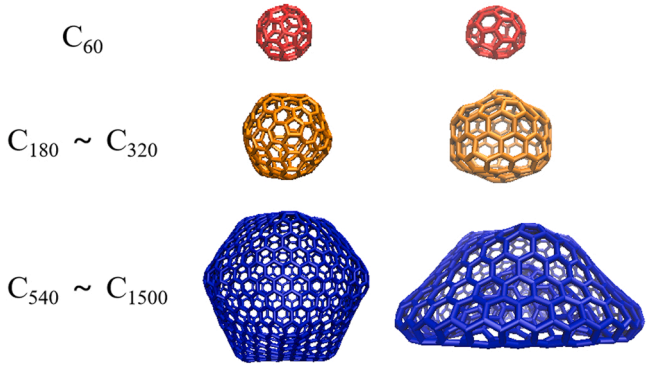

Fig. 3. Three types of buckling deformation of fullerene during impact. Left: the initial state of fullerenes before impact and Right: the state of fullerene at maximum deformation after impact.

fullerene more “elastic”. The configuration state of type III appears in C_{540} ~ C_{1500}, forming a buckled cap in the bucking state with a large volume shrinkage rate. Yang et al. [44] also revealed that the same energy absorption and dissipation mechanism exists in carbon nanotubes.

Table 2 shows the SEA of various fullerenes during impact. For a larger fullerene, a lower kinetic energy loss per unit mass of fullerene was observed. When compared to the buckling characteristics of fullerenes in type I and type II categories, type III fullerenes have a buckled cap and are more “elastic” in nature. This implies that more kinetic energy is converted into potential energy, thereby enabling them to reach a higher potential energy state. The buckled cap in type III fullerenes will interact with the carbon atoms on the top of the fullerenes due to van der Waals force [45]. Similar competitive elastic and adhesive interactions have also been observed in the deformation behavior of carbon nanotube arrays [46]. In the rebound phase, all three types of fullerenes return to their original shape and restored to the minimum potential energy state.

When fullerene hits the graphene sheet and makes contact, the fullerene will undergo local contact deformation. And a pressure distribution is generated, resulting in dynamic deformation of the bottom of the fullerene, and a buckled cap is formed. The potential energy of the system in the buckling state is higher, and the impact kinetic energy is dissipated. This implies that large-size fullerenes can act as a protective "buffer" device, with several potential applications. For example, inorganic fullerene-like nanoparticles are used as reinforcing fillers due to their high impact resistance [47], and fullerenes can be used as a drug delivery carrier to offer a robust shell [48].

Table 2
Specific energy absorption (SEA) of various fullerenes during impact.

Fullerene	C_{60}	C_{180}	C_{240}	C_{320}	C_{540}	C_{960}	C_{1500}
SEA (J/g)	4208	4111	4159	4006	3777	3618	3569

3.2. *Fracture perforation of graphene under C_{180} projectile impact*

To study the dynamics of graphene perforation under impact load, a single layer graphene with a size of 20 nm × 20 nm is considered. For the projectile, it is considered to be a rigid C_{180} fullerene structure with a varying initial velocity ranging from 3.5 km/s to 5.25 km/s. Because the mass of C_{180} projectile is relatively low ($M = 3.58 \times 10^{-21}$ g), it is considered that high impact velocity can enhance the perforation effect. The projectile is treated as a rigid body to prevent it from rupturing and collapsing before impacting the graphene sheet. During the impact, the displacement, velocity, and kinetic energy of the fullerene projectile are monitored and recorded [42]. Different from findings presented in Ref. [42], we focused on the relative state between the projectile and graphene, especially when the projectile sticks to graphene sheet, and the formation process of cracks and cone waves is further analyzed.

Figs. 4–6 show the time history of displacement, velocity, and kinetic energy of the rigid projectile, respectively. It can be seen from Fig. 4, for projectiles with a velocity less than 4.5 km/s, the displacement increases first and then decreases, and the projectile rebounds. When the projectile velocity is higher than 4.75 km/s, the displacement increases, and the projectile punches the graphene. It can be seen from Fig. 5 when the projectile velocity is less than 4.25 km/s, the velocity begins to decrease rapidly after contacting with graphene. We also observed that the different velocity curves almost coincide, indicating that under the impact of projectiles with velocities below a certain value, graphene can

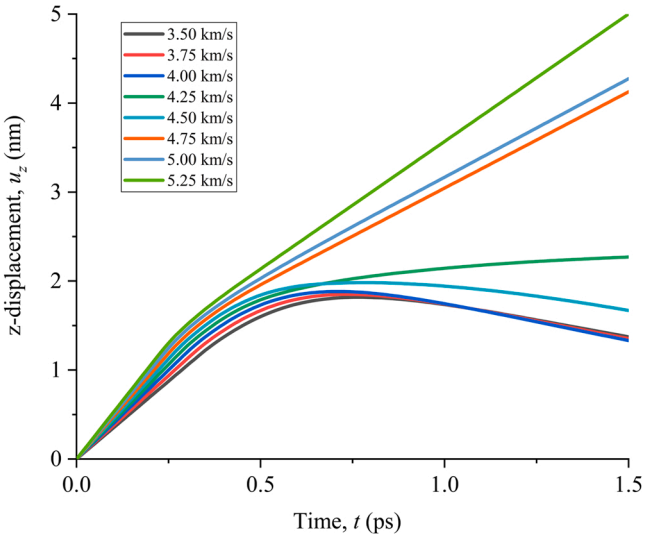

Fig. 4. Displacement-time history of fullerene projectile during impact.

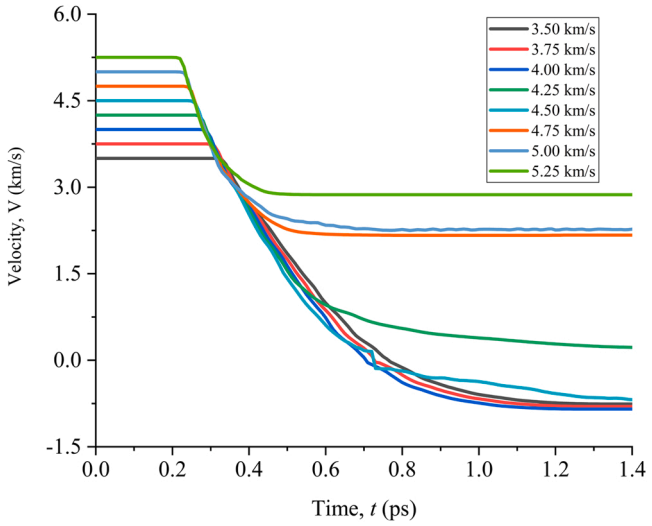

Fig. 5. Velocity-time history of fullerene projectile during impact.

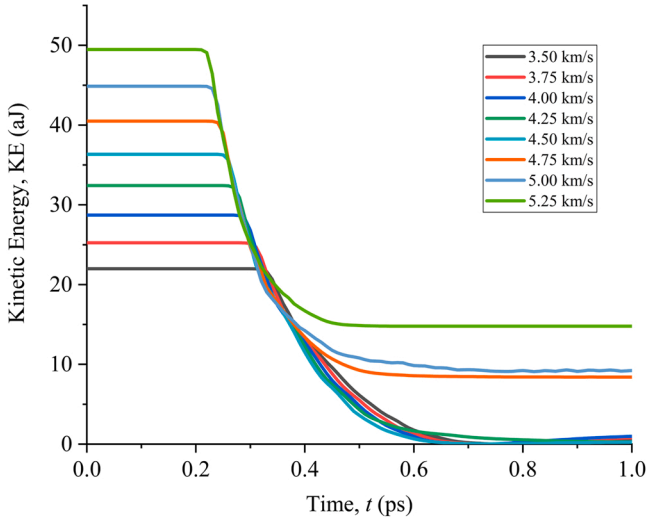

Fig. 6. Kinetic energy-time history of fullerene projectile during impact.

quickly dissipate its energy until the velocities decrease to 0, and then the projectiles rebound (the rebound velocities of the projectiles are almost equal).

As the impact continues, the projectile velocity decreases to a value of zero before increasing gradually within the negative range, corresponding to the upward movement of the projectile when it began to rebound. The velocity of projectile with various initial velocity after rebound is almost the same and the value is small. On the other hand, when the projectile velocity is greater than or equal to 4.75 km/s, the velocity decreases in different degrees during the impact contact process, and the time of contact process is very short. Following this, the projectile maintained a constant velocity, which is corresponding to the downward motion state of the projectile when perforation occurs. It is worth mentioning that the velocity-time curve of the projectile with a velocity of 4.25 km/s is different from that of other projectiles, and its velocity is almost kept near zero after impact. This is a special state – "stick", which will be further analyzed.

The cone wave formation, crack initiation and propagation and damage mode of graphene sheet is studied by Haque et al. [42]. Figs. 7–9 shows projectiles with velocity of 4 km/s, 4.5 km/s and 5 km/s at different time, respectively.

(I) When the velocity of the fullerene projectile is less than 4.25 km/s, the projectile rebounds. As shown in Fig. 7, the fullerene projectile has just begun to maintain a constant velocity impact on the graphene below. At 0.5 ps, the impact contact occurs, and the large deformation of the graphene is conical. With the continuation of the impact process, the conical deformation of the graphene is increasing, and the conical wave propagates outward.

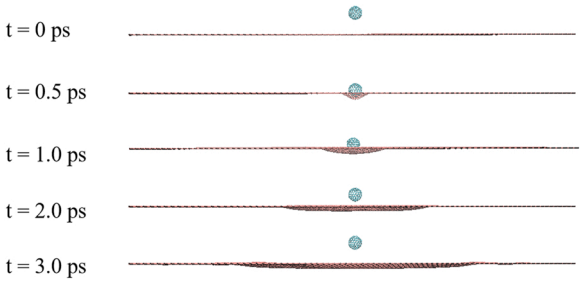

Fig. 7. Process of graphene impacted by projectile with 4 km/s.

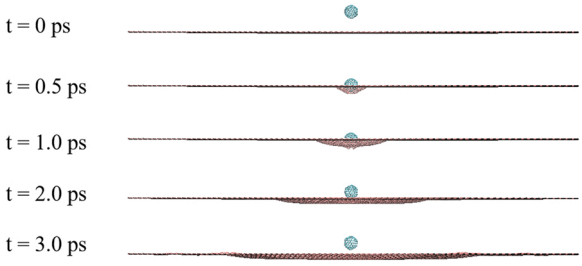

Fig. 8. Process of graphene impacted by projectile with 4.5 km/s.

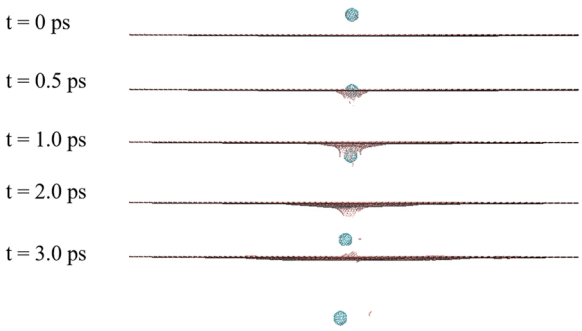

Fig. 9. Process of graphene impacted by projectile with 5 km/s.

(II) When the velocity of fullerene projectile is between 4.25 km/s and 4.75 km/s, projectile sticks. As shown in Fig. 8, when the projectile is far from the target, the target attempts to absorb the far projectile. As the projectile approaches the target, the van der Waals force between the projectile and the target changes from attractive force to repulsive force. After reaching a certain relative distance (depending on the physical and geometric characteristics of the system), the rejection is overcome, and there are two possible occurrences: the projectile is either rebounds or trapped by the target. After the projectile impacts with the target graphene, the projectile does not rebound immediately, but sticks to the graphene, as shown in Fig. 10. This means that graphene has the ability to capture the projectile in a certain speed range, and graphene can dissipate the kinetic energy of the projectile. This property is of great significance for the development of graphene into impact resistant materials.

(III) When the velocity of the fullerene projectile is greater than 4.75 km/s, projectile perforates. As shown in Fig. 9, cracks appear in a short contact time between the fullerene projectile and graphene. At the

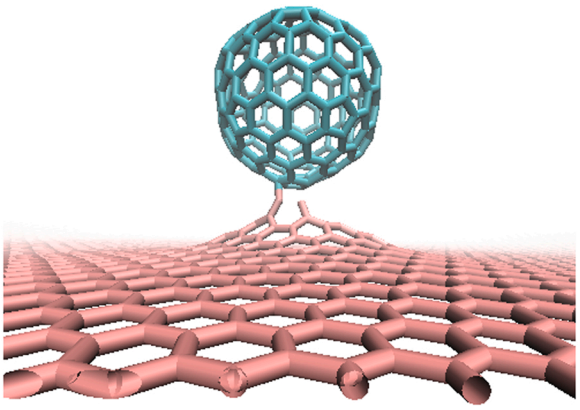

Fig. 10. Projectile sticks to the grapheme.

center of the impact area, a small amount of carbon atoms is sputtered. Then, the response is rapidly amplified in the form of concentric progressive waves and propagates from the contact point to the boundary. Then the wave is reflected by the boundary and forms a composite state of displacement composed of multiple excitation modes. With the continuous impact process, the projectile continues to go down, and perforation occurs. More carbon atoms are sputtered, holes are formed, and the projectile still maintains high velocity after perforation. Compared with unperforated graphene, perforated graphene has smaller cone pits because most of the energy is converted into carbon-carbon bond cleavage. It can be seen from the diagram that when the projectile passes the graphene, local deflection occurs at the contact point, and the velocity of the projectile is no longer vertical downward.

The ballistic limit velocity is an important parameter for evaluating the protective performance of materials. It refers to the minimum velocity required for the projectile to completely penetrate the protective material [32,49]. When the projectile velocity is less than the ballistic limit velocity (in this case – 4.75 km/s), perforation does not occur, however the graphene deforms locally. After impact, this deformation is restored due to the elastic rebound of the graphene sheet. When the impact velocity is higher than the ballistic limit velocity (4.75 km/s), the graphene will be perforated. At high impact velocity, cracks initiate in graphene through bond fracture and propagate along the graphene. Cracks propagate to a large extent due to membrane tension load. The boundary contour of the conical wave can be clearly seen from Figs. 11 and 12, and the cone wave shows a symmetrical semicircle. Fig. 13 shows that the cone wave forms a composite state of displacement composed of multiple excitation modes due to the perforation of graphene. As shown in Figs. 11–13, a clear tensile stress wave is found around the impact zone, which quickly spread to the rest of the material. After penetration, the energy release around the perforation crack leads to the continuous growth of the crack.

Fig. 14 shows the crack mode of a graphene sheet under impact by fullerene projectiles with different velocities. When the projectile velocity is equal to 4.25 km/s, the projectile rebounds without perforating the graphene sheet, but leads to the formation of cracks in the graphene sheet. For projectiles with velocities below 4.75 km/s, graphene experienced extensive elastic deformation before crack initiation and propagation. However, when the velocity exceeds 4.75 km/s, the impact zone ruptures immediately when the projectile approaches graphene, resulting in a large number of suspended bonds and carbon atoms sputtering. It can be seen from Fig. 14 (a)-(d), with the increase of impact velocity, the number of cracks increases from one to four, the total length of cracks also increases, more carbon-carbon bonds break during the initiation and propagation of cracks, and more energy is dissipated. For all crack modes, the crack with an angle around 60°, 90°, 120° and 180° between each other, which are in good agreement with the results obtained in the microballistic test conducted by Lee et al. [28]. These observed crack angles are related to the hexagonal periodic arrangement of carbon atoms in graphene [50].

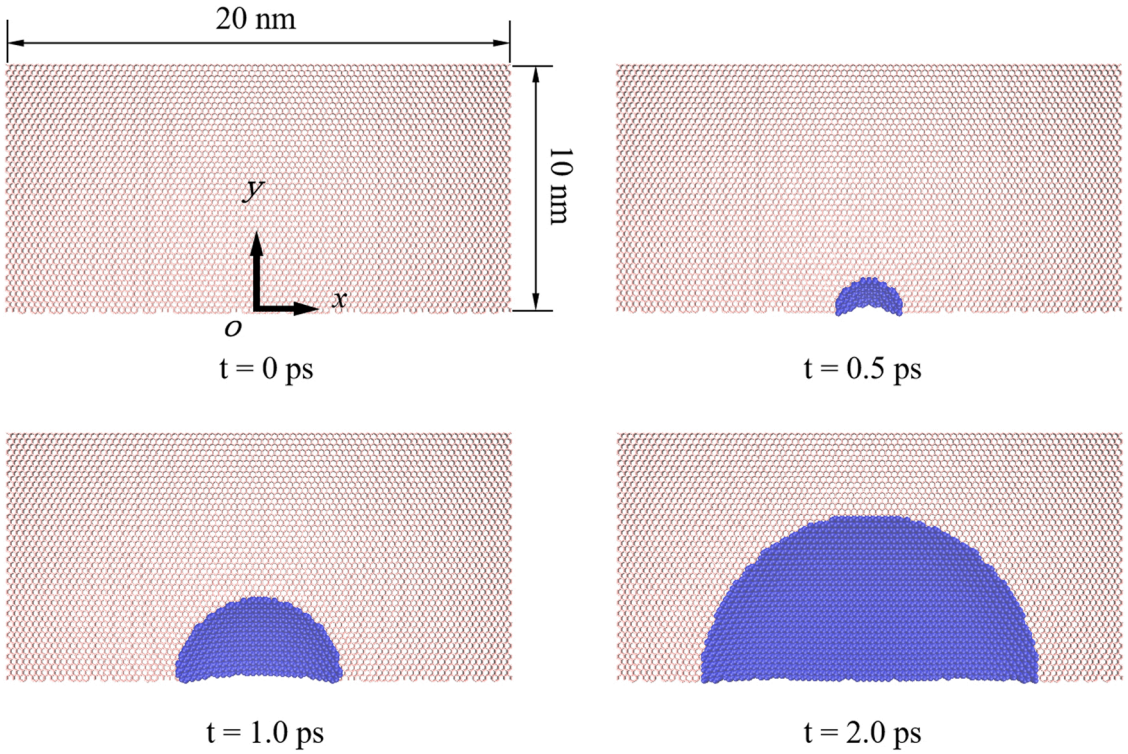

Fig. 11. Cone wave formation process of graphene impacted by projectile (C_{180}) with 4 km/s. (The blue regions represent the wave propagation area).

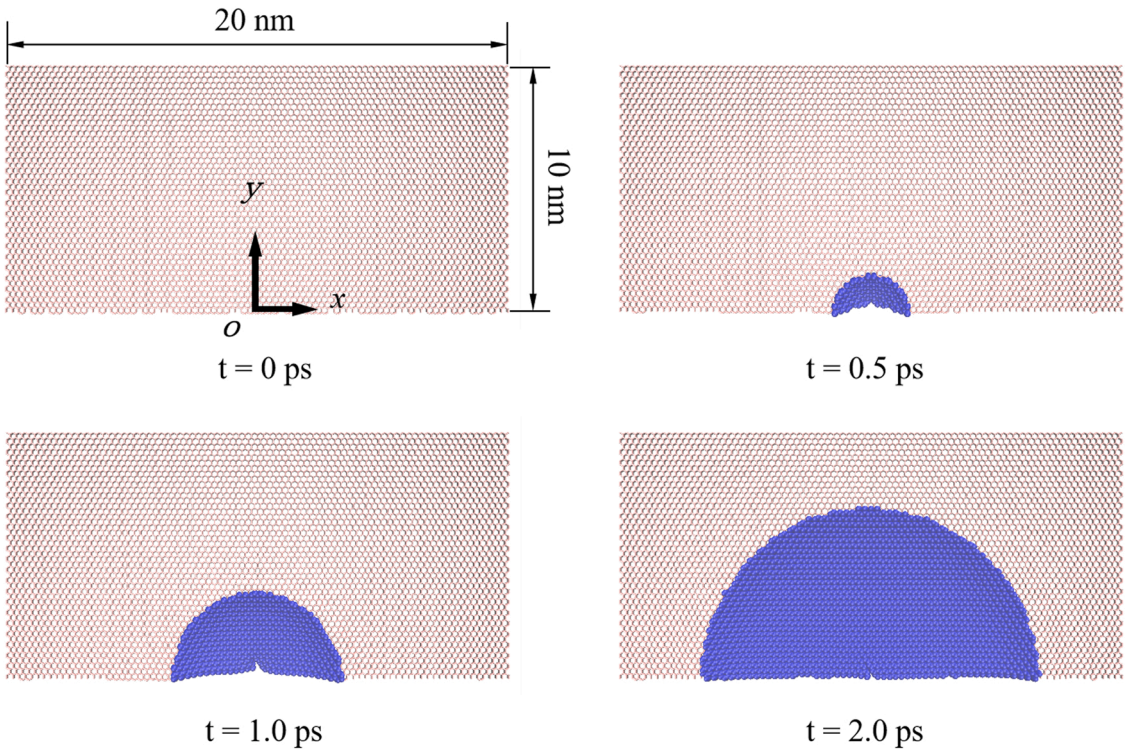

Fig. 12. Cone wave formation process of graphene impacted by projectile (C_{180}) with 4.5 km/s. (The blue regions represent the wave propagation area).

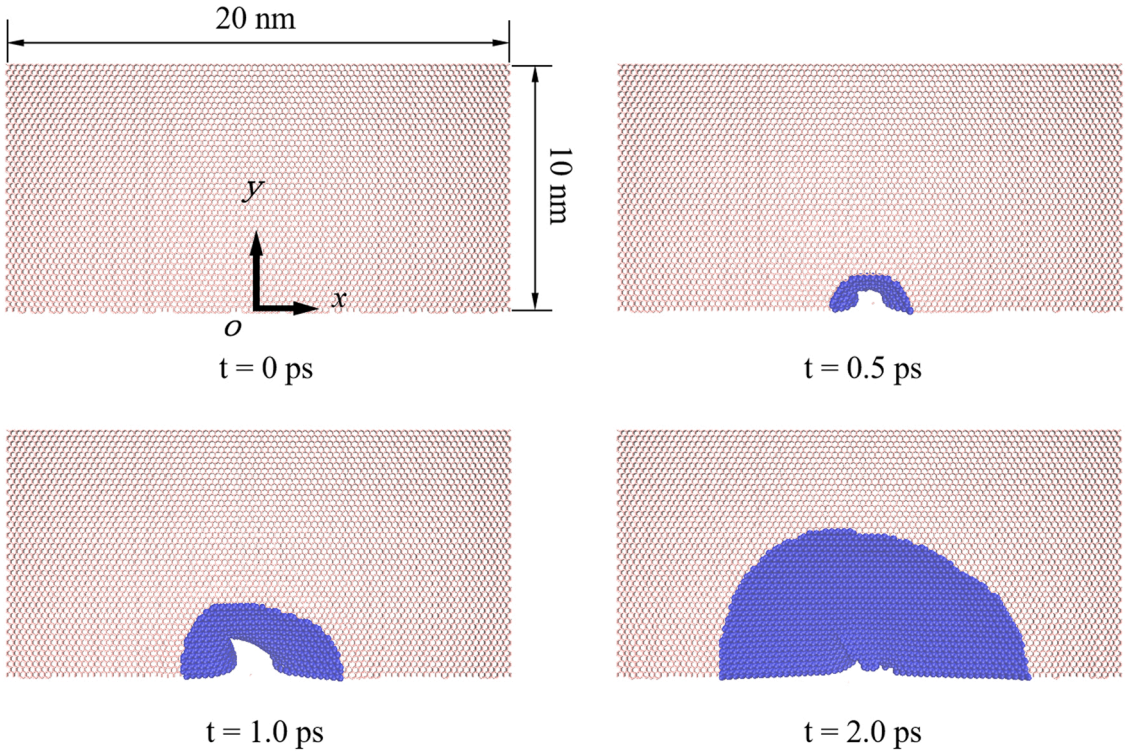

Fig. 13. Crack formation process of graphene impacted by projectile (C_{180}) with 5 km/s. (The blue regions represent the wave propagation area).

3.3. Effect of fullerene projectile size and initial velocity on ballistic limit velocity

So far, most of the existing simulation research in literature only involves the study of the ballistic limit velocity of a certain fixed-size projectile [30–32,42]. In this section, the combined effects of varying fullerene projectile sizes and velocities on the impact behaviors of a graphene sheet with dimensions 20 nm × 20 nm are investigated. The numerical simulation setup is the same as the configuration illustrated in Fig. 1. The fullerenes are considered to be rigid and non-deformable in

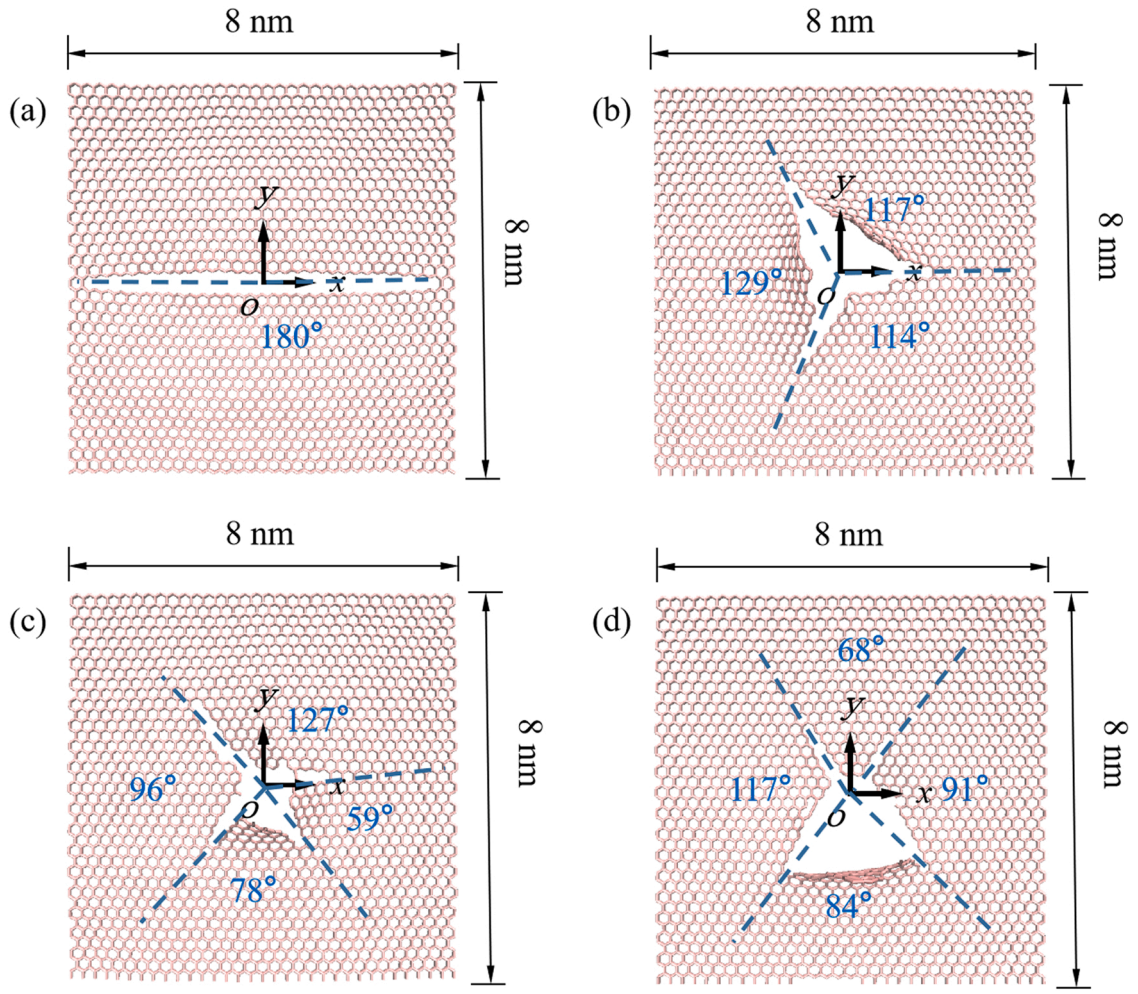

Fig. 14. Crack mode of graphene under impact by fullerene projectiles (C_{180}) with different velocities (partial drawing). (a) 4.25 km/s, (b) 4.75 km/s, (c) 5 km/s, and (d) 5.25 km/s.

our simulations to avoid the fracture and disintegration of the projectiles during impact. Fig. 15 shows the effect of fullerene projectile sizes and initial velocities on the residual velocities of projectiles. Based on the observed residual velocities, the states of graphene under impact by fullerene projectiles with different velocities can be divided into three cases.

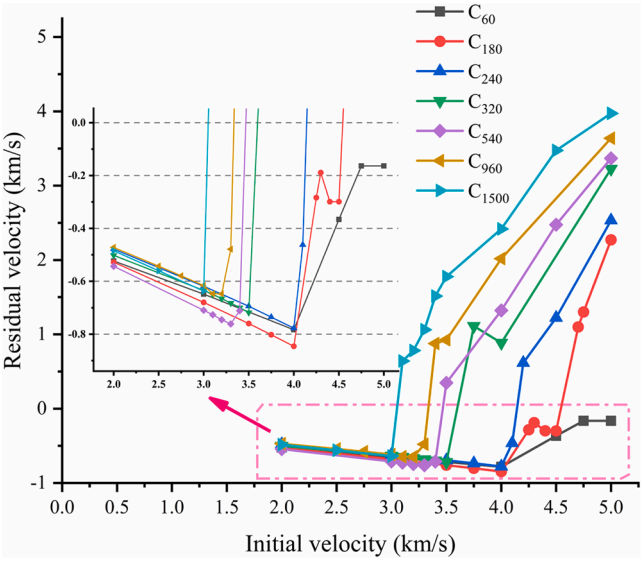

Fig. 15. Plot of residual velocity against initial velocity of fullerene projectiles with different sizes.

(I) When the initial velocity is low (below 3 km/s), the fullerene projectile cannot penetrate graphene and it rebounds with a negative residual velocity. The residual velocity increases with an increase in the initial velocity, however, the residual velocity value remains very low, which implies that most kinetic energy is dissipated by graphene.

(II) As the initial velocity increases (between 3 and 4 km/s), the value of the residual velocity changes from negative to positive. Small-size fullerene projectiles (C_{60} ~ C_{240}) are captured by graphene in this velocity range, and the velocity becomes zero. All kinetic energy is absorbed by graphene, which is due to the formation of new carbon-carbon bond between fullerene projectile and graphene, and fullerene projectile sticks to graphene. Large-size fullerene projectiles (C_{320} ~ C_{1500}), with greater kinetic energy and volume, were not captured and they penetrated the graphene sheet at a very low speed.

(III) When the initial velocity exceeds the ballistic limit velocity, the impact zone ruptures immediately as the projectile approaches the graphene, and the fullerene projectile penetrates the graphene, resulting in a large number of suspended bonds and carbon atoms sputtering. It can be seen from Fig. 15, after perforation, the initial and residual velocities are almost linear, and the value of the residual velocity is relatively large.

Fig. 16 shows that the ballistic limit velocity decreases with the

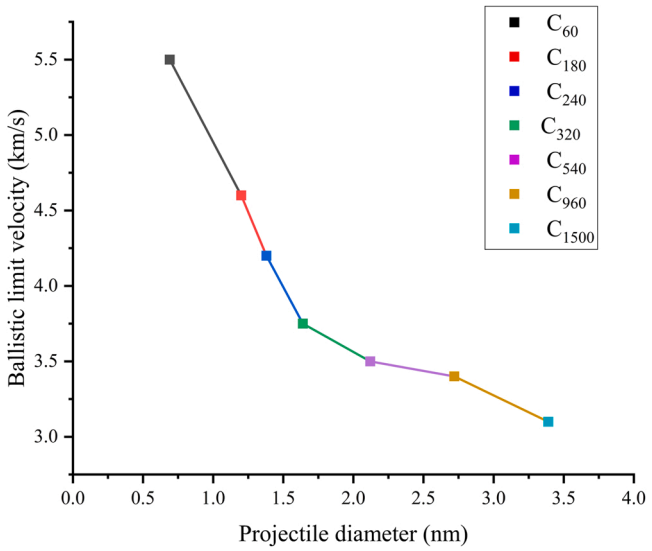

Fig. 16. Plot of ballistic limit velocity against projectile diameter.

increase of the fullerene projectile size. We observed that projectile size change has a greater impact on the limit velocity, however, as the projectile size continues to increase, the limit velocity becomes less sensitive to the size change, and the reduction in the ballistic limit velocity also becomes negligible. Similar to space return capsules, the suitability of large-size fullerene projectile as a protective shield for impactor is greatly enhanced by their high limit speed and a relatively larger internal space.

4. Conclusions

In this work, the MD simulation method is used to conduct a comprehensive study on the buckling characteristics, perforation behavior, crack mode, and ballistic limit velocity in fullerene-graphene sheet impact system. Buckling characteristics of fullerenes during impact can be divided into three categories among which large-size fullerene forms a buckled cap after impact, leading to better kinetic energy absorbing ability. These observations show that large-size fullerenes can be used as a protective structural material (or "buffer") for impactor. Furthermore, our simulation results revealed that when graphene sheet is impacted by C_{180} projectile with different velocities, the C_{180} projectile rebounded at low velocity, sticked to graphene at high velocity, and perforated the graphene sheet at higher impact velocity. In addition, our results clarified the effect of fullerene projectile size and initial velocity on their ballistic limit velocities. These observations can provide guidance for the geometric design of fullerene as an impact protector or shield. Overall, our results show that graphene and fullerene have great potential as impact protection materials.

CRediT authorship contribution statement

Yang Zhang: Investigation, Resources, Supervision, Writing - original draft. **Yun Qiu:** Conceptualization, Formal analysis, Software, Validation, Writing – original draft. **Fuzhou Niu:** Validation, Visualization, Writing – review & editing. **A.S. Ademiloye:** Investigation, Validation, Supervision, Writing – review & editing.

Declaration of Competing Interest

The authors declare that they have no known competing financial interests or personal relationships that could have appeared to influence the work reported in this paper.

Data availability

The data that support the findings of this study are available from the corresponding author, A.S. Ademiloye, upon reasonable request.

Acknowledgments

This work was supported in part by National Natural Science Foundation of China under Grant No. 11902159 and No. 61903269, Swansea University New Faculty Grant, and the Hong Kong Scholars Program (Project No. XJ2019016).

References

[1] D.A. Shockey, J.W. Simons, D.R. Curran, The damage mechanism route to better armor materials, Int. J. Appl. Ceram. Technol. 7 (5) (2010) 566–573.
[2] A. Cabrilo, K. Geric, Weldability of high hardness armor steel, Adv. Mater. Res. 1138 (2016) 79–84.
[3] E. Grossman, I. Gouzman, R. Verker, Debris/micrometeoroid impacts and synergistic effects on spacecraft materials, MRS Bull. 35 (1) (2010) 41–47.
[4] J.C. Liou, N.L. Johnson, Planetary science. Risks in space from orbiting debris, Science 311 (5759) (2006) 340–341.
[5] K.S. Novoselov, et al., Electric field effect in atomically thin carbon films, Science 306 (5696) (2004) 666–669.
[6] T. Zhang, et al., Flaw insensitive fracture in nanocrystalline graphene, Nano Lett. 12 (9) (2012) 4605–4610.
[7] S.W. Cranford, When is 6 less than 5? Penta- to hexa-graphene transition, Carbon 96 (2016) 421–428.
[8] Steven, et al., Mechanical properties of graphyne, Carbon 49 (13) (2011) 4111–4121.
[9] C. Lee, et al., Measurement of the elastic properties and intrinsic strength of monolayer graphene, Science 321 (5887) (2008) 385–388.
[10] P.J. Hogg, Composites in armor, Science 314 (5802) (2006) 1100–1101.
[11] W. Liu, et al., Influence of different back laminate layers on ballistic performance of ceramic composite armor, Mater. Des. 87 (2015) 421–427.
[12] A.K. Geim, K.S. Novoselov, The rise of graphene, Nat. Mater. 6 (3) (2007) 183–191.
[13] C. Xi, Y. Huang, Nanomechanics modeling and simulation of carbon nanotubes, J. Eng. Mech. 134 (3) (2016) 211–216.
[14] J.H. Lee, et al., Dynamic mechanical behavior of multilayer graphene via supersonic projectile penetration, Mater. Sci. 346 (6213) (2014) 1092–1096.
[15] N. Kaur, et al., Behaviour of a bucky-ball under internal and external pressures, Physics (2007) 1017–1022.
[16] J.H. Lee, et al., High strain rate deformation of layered nanocomposites, Nat. Commun. 3 (2012) 1164.
[17] M. Grujicic, et al., A computational analysis of the ballistic performance of light-weight hybrid composite armors, Appl. Surf. Sci. 253 (2) (2006) 730–745.
[18] M. Colakoglu, O. Soykasap, T. Zek, Experimental and numerical investigations on the ballistic performance of polymer matrix composites used in armor design, Appl. Compos. Mater. 14 (1) (2007) 47–58.
[19] D.R. Ambur, et al., Numerical simulations for high-energy impact of thin plates, Int. J. Impact Eng. 25 (7) (2001) 683–702.
[20] M. Henkel, H.M. Urbassek, Ta cluster bombardment of graphite: molecular dynamics study of penetration and damage, Nucl. Instrum. Methods Phys. Res. 145 (4) (1998) 503–508.
[21] R. Chen, et al., Energy transfer under impact load studied by molecular dynamics simulation, J. Nanopart. Res. 11 (3) (2009) 589–600.
[22] M.A. Rafiee, et al., Fracture and fatigue in graphene nanocomposites, Small 6 (2) (2010) 179–183.
[23] Y. Cui, S.I. Kundalwal, S. Kumar, Gas barrier performance of graphene/polymer nanocomposites, Carbon 98 (2016) 313–333.
[24] Y. Xu, A.S. Fleischer, G. Feng, Reinforcement and shape stabilization of phase-change material via graphene oxide aerogel, Carbon 114 (2017) 334–346.
[25] S. Haghighi, R. Ansari, S. Ajori, A molecular dynamics study on the interfacial properties of carbene-functionalized graphene/polymer nanocomposites, Int. J. Mech. Mater. Des. 16 (2) (2020) 387–400.
[26] Z. Zhao, et al., Geometrically nonlinear bending of functionally graded nanocomposite trapezoidal plates reinforced with graphene platelets (GPLs), Int. J. Mech. Mater. Des. 15 (4) (2019) 791–800.
[27] A.F. Ávila, A.S. Neto, H. Nascimento Junior, Hybrid nanocomposites for mid-range ballistic protection, Int. J. Impact Eng. 38 (8) (2011) 669–676.
[28] J.H. Lee, et al., Dynamic mechanical behavior of multilayer graphene via supersonic projectile penetration, Science 346 (6213) (2014) 1092–1096.
[29] J. Xu, et al., Molecular dynamics simulation of impact response of buckyballs, Mech. Res. Commun. 49 (2013) 8–12.
[30] R.A. Bizao, et al., Scale effects on the ballistic penetration of graphene sheets, Sci. Rep. 8 (1) (2018) 6750.
[31] J. Xu, et al., Energy absorption ability of buckyball C720 at low impact speed: a numerical study based on molecular dynamics, Nanoscale Res. Lett. 8 (1) (2013) 1–10.
[32] Z. Meng, et al., Reduced ballistic limit velocity of graphene membranes due to cone wave reflection, Extrem. Mech. Lett. 15 (2017) 70–77.

[33] Y. Qiu, et al., Molecular dynamics simulations of single-layer and rotated double-layer graphene sheets under a high velocity impact by fullerene, Comput. Mater. Sci. 182 (2020), 109798.
[34] S. Plimpton, Fast parallel algorithms for short-range molecular dynamics, J. Comput. Phys. 117 (1) (1995) 1–19.
[35] W. Humphrey, A. Dalke, K. Schulten, VMD: visual molecular dynamics, J. Mol. Graph. 14 (1) (1996) 33–38.
[36] S.J. Stuart, A.B. Tutein, J.A. Harrison, A reactive potential for hydrocarbons with intermolecular interactions, J. Chem. Phys. 112 (14) (2000) 6472–6486.
[37] P. Hünenberger, Thermostat algorithms for molecular dynamics simulations, Adv. Comput. Simul. 173 (2005) 105–149.
[38] D.W. Brenner, Empirical potential for hydrocarbons for use in simulating the chemical vapor deposition of diamond films, Phys. Rev. B, Condens. Matter 42 (15) (1990) 9458–9471.
[39] A.H. Castro Neto, et al., The electronic properties of graphene, Rev. Mod. Phys. 81 (1) (2009) 109–162.
[40] Y.Y. Zhang, Q.X. Pei, C.M. Wang, Mechanical properties of graphynes under tension: a molecular dynamics study, Appl. Phys. Lett. 101 (8) (2012), 081909.
[41] S. Melchor, J.A. Dobado, CoNTub: an algorithm for connecting two arbitrary carbon nanotubes, J. Chem. Inf. Comput. Sci. 44 (5) (2004) 1639–1646.
[42] B.Z. Haque, S.C. Chowdhury, J.W. Gillespie, Molecular simulations of stress wave propagation and perforation of graphene sheets under transverse impact, Carbon 102 (2016) 126–140.
[43] R. Shorter, et al., Axial compression of hollow elastic spheres, J. Mech. Mater. Struct. 5 (5) (2010) 693–705.
[44] X. Yang, P. He, H. Gao, Modeling frequency- and temperature-invariant dissipative behaviors of randomly entangled carbon nanotube networks under cyclic loading, Nano Res. 4 (12) (2011) 1191–1198.
[45] T. Hertel, R.E. Walkup, P. Avouris, Deformation of carbon nanotubes by surface van der Waals forces, Phys. Rev. B 58 (20) (1998) 13870–13873.
[46] X. Yang, P. He, H. Gao, Competing elastic and adhesive interactions govern deformation behaviors of aligned carbon nanotube arrays, Appl. Phys. Lett. 101 (5) (2012), 053105.
[47] M. Naffakh, et al., Opportunities and challenges in the use of inorganic fullerene-like nanoparticles to produce advanced polymer nanocomposites, Prog. Polym. Sci. 38 (8) (2013) 1163–1231.
[48] R.D. Bolskar, Fullerenes for drug delivery, in: B. Bhushan (Ed.), Encyclopedia of Nanotechnology, Springer, Netherlands: Dordrecht, 2016, pp. 1267–1281.
[49] P.M. Cunniff, A semiempirical model for the ballistic impact performance of textile-based personnel armor, Text. Res. J. 66 (1) (1996) 45–58.
[50] J. Hou, et al., Magic auxeticity angle of graphene, Carbon 149 (2019) 350–354.